Optics and Laser Technology 99 (2018) 396–401

Contents lists available at ScienceDirect

Optics and Laser Technology

journal homepage: www.elsevier.com/locate/optlastec

Full length article

Refractive index sensor based on lateral-offset of coreless silica interferometer

Nur Faizzah Baharin, Asrul Izam Azmi *, Ahmad Sharmi Abdullah, Muhammad Yusof Mohd Noor

Department of Communication Engineering, Faculty of Electrical Engineering, Universiti Teknologi Malaysia, 81310 Skudai, Johor, Malaysia

ARTICLE INFO

Article history:
Received 24 April 2017
Received in revised form 12 September 2017
Accepted 12 September 2017
Available online 22 September 2017

Keywords:
Fiber interferometer
Symmetrical offset
Coreless-silica fiber
Refractive index sensor

ABSTRACT

A compact, cost-effective and high sensitivity fiber interferometer refractive index (RI) sensor based on symmetrical offset coreless silica fiber (CSF) configuration is proposed, optimized and demonstrated. The sensor is formed by splicing a section of CSF between two CSF sections in an offset manner. Thus, two distinct optical paths are created with large index difference, the first path through the connecting CSF sections and the second path is outside the CSF through the surrounding media. RI sensing is established from direct interaction of light with surrounding media, hence high sensitivity can be achieved with a relatively compact sensor length. In the experimental work, a 1.5 mm sensor demonstrates RI sensitivity of 750 nm/RIU for RI range between 1.33 and 1.345. With the main attributes of high sensitivity and compact size, the proposed sensor can be further developed for related applications including blood diagnosis, water quality control and food industries.

1. Introduction

Optical fiber sensors have been continuously researched to satisfy the ever growing challenges in real applications. Optical fiber based sensor is desirable for many applications due to its compactness, and high design flexibility. There are different types of fiber based sensing techniques which may categorized into fiber laser [1], fiber Bragg grating [2] and fiber interferometer [3–17]. Fiber interferometers such as Fabry-Perot interferometer (FPI) [3], Michelson interferometer (MI) [4] and Mach-Zehnder interferometers (MZI) [5–17] are typically realized from combination of different segments of optical fibers jointed by fusion splicing process. The sensors can be optimized for single or multi-parameters sensing to detect measurands such as temperature, refractive index (RI), bending, displacement and vibration. In order to realize a MZI i.e. with light split and recombine mechanisms, few methods have been proposed which include fiber tapers [5,6], fiber core mismatched [7], partially ablated fiber using femtosecond laser [8–10], peanut-shape structure [11], collapsed region in photonic crystal fiber (PCF) [12,13], lateral-offset [14–17]. Fiber tapers technique has been demonstrated to achieve high sensitivity in refractive index sensing with reported result of 1656.35 nm/RIU for a tapered SMF [5] and 2210.85 nm/RIU for tapers incorporated in a thinned SMF [6]. Ultra-compact partially ablated fiber technique using femtosecond laser has shown further enhancement of performance with achieved sensitivity as high as ~10,000 nm/RIU [8]. The use of PCF for refractive index sensing also has gained promising result of 1600 nm/RIU with relatively low temperature dependency of 8.49 pm/°C [13]. However, all of the previously mentioned techniques require the use of special equipment or fiber which inevitably will increase overall fabrication cost.

Meanwhile, lateral-offset technique is relatively simpler in terms of process and equipment used compared with the aforementioned techniques. There are several noteworthy works related to lateral-offset fiber interferometer have been demonstrated which can be categorized into two major types. The first type requires a small lateral offset of the sensing fiber such that light from a lead-in fiber will be spread into core and cladding of the sensing fiber, and hence detection is established from the interaction between the cladding modes with the surrounding material [14–16]. The second type of the technique requires large offset of sensing fiber such that light from the lead-in fiber will be spread into the surrounding (e.g. air and liquid) as well as the cladding of a fiber [17], which creates two distinct interferometer arms with large RI difference. RI sensitivity of the latter technique is significantly higher than the former, which can be achieved with relatively much shorter sensor length attributed from direct interaction with the surrounding material. For example, the sensitivity achieved by large offset sensor has been reported as high as 3402 nm/RIU with arm length ~0.41 mm [17]. This sensitivity is much higher compared to the short offset sensor, for example, a

* Corresponding author.
E-mail address: asrul@utm.my (A.I. Azmi).

https://doi.org/10.1016/j.optlastec.2017.09.028
0030-3992/

small offset evanescent field type sensor with the length of 66 mm has achieved sensitivity of −26.22 nm/RIU [14]. A subsequent work in core-offset evanescent type sensor with tapered MZI arm has shown improvement with reported sensitivity of 78.7 nm/RIU with relatively shorter sensor length of 30 mm [16].

As stated previously, a large offset technique with direct interaction mechanism has demonstrated high sensitivity (in the range of thousands of nm/RIU) with relatively short sensor length. However, the use of single mode fiber as the sensing element and lead in/out fiber in direct interaction scheme [17] is subjected to high tolerance requirement as the core diameter of single mode fiber is typically around 9 μm. This suggests that slight misalignment in the range of few micrometers could lead to an unworkable sensor. To mitigate this problem, we propose the use of core-offset structure based on coreless silica fiber (CSF) in MZI configuration. The use of CSF allows lower tolerance requirement due to the large diameter of the lead in/out cladding of 125 μm, hence easier fabrication while retaining high sensitivity of the scheme. In this work, the sensor structure is simulated in BeamProp software to obtain the optimum offset value for maximum fringe for a particular arm length. The optimized designs are then fabricated using customized fusion splicing recipe. A CSF based MZI sensor with length of 1.5 mm demonstrates RI sensitivity of 750 nm/RIU for the range between 1.33 and 1.345. Temperature dependence of the sensor is also studied to understand the extent of temperature effect. Temperature sensitivity manifested by the sensor is 27.21 pm/°C for the range between 30 and 100 °C. The main advantages of this sensor are that, high sensitivity has been achieved with relatively very short sensor length of 1.5 mm and the lower tolerance in term of the accuracy requirement of offset distance that reduce the complexity during fabrication process.

2. Working principle and optimization

The proposed MZI structure consists of three sections of CSFs (FG125LA, Thorlabs) sandwiched between two lead in/out SMFs as shown in Fig. 1. All the fiber sections are aligned centrally in the y-direction. Meanwhile, in the x-direction, section B is offset by a certain distance, d relative to the position of the top of sections A and C. This creates a symmetrical structure of the sensor which aimed to simplify the optimization process by only varying the offset distance at particular sensor length (section B length). The second optical path is created in a gap between section A and C from the offset process, allowing light to be directly interact with surrounding refractive index. As can be seen, reflected light from Section A and Section C of the CSF may recombine to form a Fabry-Perot structure. However, the weak reflection from Section C in current setup prevents the desired interference effect from occur. The core/cladding diameters of SMF used in simulation and experiment are 9 μm/125 μm, while the cladding diameter of CSFs is 125 μm. Section A, B and C lengths are 0.5 mm, 1.5 mm and 0.5 mm, respectively. The use of a 125 μm diameter of the CSF which is identical to the SMF is to avoid unnecessary complexity in splicing process.

As illustrated in Fig. 1, the incoming light is spread throughout the CSF diameter of the section A. Due to the offset, the light is split into the surrounding and into section B, and then recombined at section C. A large portion of light in section C is further transmitted to the cladding of the lead-out fiber. The cladding mode in SMF will be eventually diminished due to high scattering loss of the cladding and leakage loss. Leakage loss occurs if the cladding surface is covered by material with refractive index higher than that of the cladding such as acrylic residue [18]. Due to small overlap of surface area, a small portion of the light in section C is transferred to core of the lead-out SMF. The working principle of the proposed structure is identical to a MZI. Hence, the intensity of the light detected at the receiving photo detector can be expressed as:

$$I(\lambda) = I_1 + I_2 + 2\sqrt{I_1 I_2}\cos\emptyset \quad (1)$$

I_1 and I_2 are the light intensities of the CSF modes and the gap modes, respectively. While $\emptyset$ is the phase difference between these two modes which can be written as:

$$\emptyset = \left(\frac{2\pi(n_{cl} - n_{eff})L_0}{\lambda}\right) \quad (2)$$

where λ is center wavelength of light source, L_o is the MZI arm length, n_{cl} and n_{eff} are the effective refractive indices of CSF cladding and surrounding material in the gap, respectively. Any change of the surrounding RI will drastically change the interference spectrum due to direct interaction of the light with the surrounding. According to this equation, it is crucial to have $I_1 = I_2$ in order to get maximum fringe visibility of the interference spectra [19]. The dip and peak of the interference spectra occur when the $\emptyset$ is multiple of $(2N + 1)\pi$ and $2N\pi$, respectively, where N is an integer. Under this

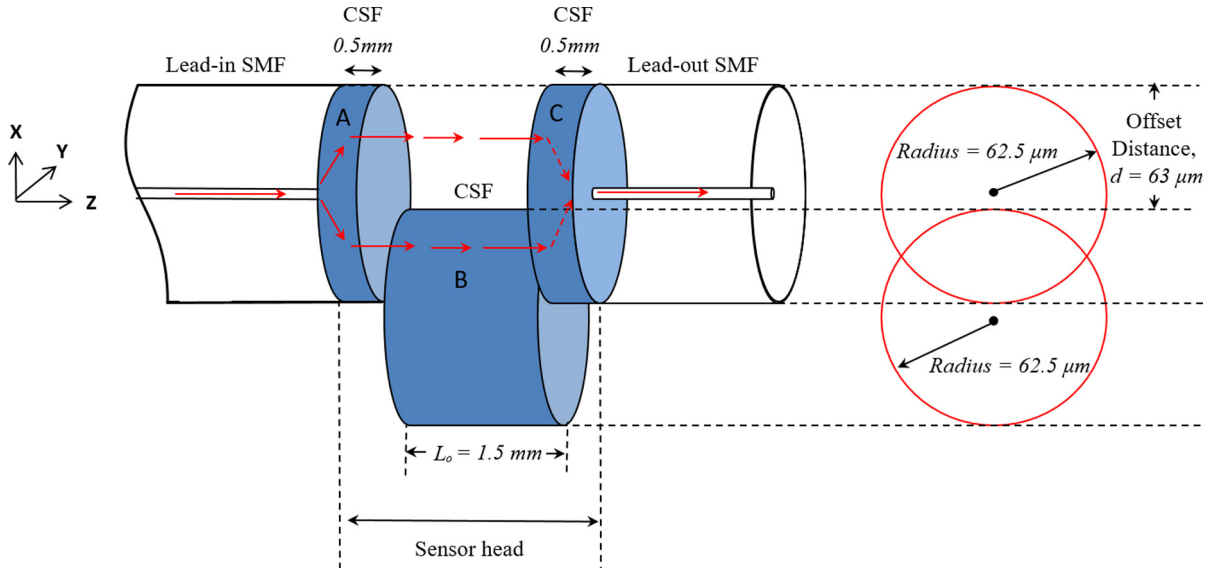

Fig. 1. Schematic of the core-offset CSF based MZI sensor.

circumstance, the dip wavelength in the interference spectra is observable at this condition:

$$\lambda_{dip} = \frac{2(n_{cl} - n_{eff})L_0}{(2N+1)} \tag{3}$$

Meanwhile, the free spectral range (FSR) between two successive transmitted λ of the structure is given by:

$$FSR = \frac{\lambda^2}{(n_{cl} - n_{eff})L_0} \tag{4}$$

From Eq. (3), the sensitivity of the dip wavelength to the change of surrounding RI can be obtained as:

$$\Delta\lambda_{dip} = -\frac{2L_0}{(2N+1)}\Delta n_{eff} \tag{5}$$

From Eq. (5), it is apparent that the RI sensitivity is proportional to the surrounding RI change and sensor length.

Light that transmitted through the surrounding media that creates the second optical path will undergo partial reflection at glass-surrounding media interface and surrounding media-glass interface. Assuming the light incident perpendicular to the surface, the fraction of light reflected at the surface, r may be computed using the Fresnel equation:

$$r = \left(\frac{n_{cl} - n_{eff}}{n_{cl} + n_{eff}}\right)^2 \tag{6}$$

The loss due to Fresnel reflection can be determined from $-10\log_{10}(1-r)$ dB. In addition, the surrounding media that creates a longitudinal offset between Section A and C also incur an additional loss. Since coupling efficiency is proportional to the overlapped factor between two adjacent media [20], the lateral offset of Section B causes significant change in coupling efficiency between two fiber sections or between fiber and surrounding media. Angular misalignment of the in-line fibers that unintentionally introduced (although not visible) during fabrication will incur more loss of the desired signal.

The MOST optimizer in BeamPROP software is used to simulate the transmission spectra of the sensor in order to determine the offset for maximum fringe visibility. Fringe visibility for different sensor lengths of 0.5 mm, 1.0 mm and 1.5 mm are investigated by varying the offset distance. In the simulation, the background index is set to 1.33 while the RI of CSFs is set to 1.444 according to the manufacturer specification [21]. The operation of the sensor is evidently indicated from field distribution observed shown in Fig. 2(a). The plot of maximum fringe visibility against the offset distance for three different arm lengths indicated in Fig. 2(b) reveals that there is an optimum offset distance at a particular sensor length. The simulated spectra for all lengths with optimum offset distance are indicated in Fig. 2(c). This sensor offers lower tolerance in term of the offset accuracy due to large diameter of CSF. Thus, fringe visibility for sensor sample 1.5 mm is distinguishable within large offset range from 50 to 70 μm (more than 20 μm offset range) as shown in Fig. 2(d). This range may not possible by using SMF (from the previous technique in [17]) as the SMF core may be completely out of overlapping position. The optimum offset for each sensor length determined from simulation is summarized in Table 1.

Table 1
Optimum offset distance for each sensor sample.

Sample	MZI Arm length, *Lo* (mm)	Optimum offset distance, *d* (μm)
1	0.5	60.5
2	1.0	62.0
3	1.5	63.5

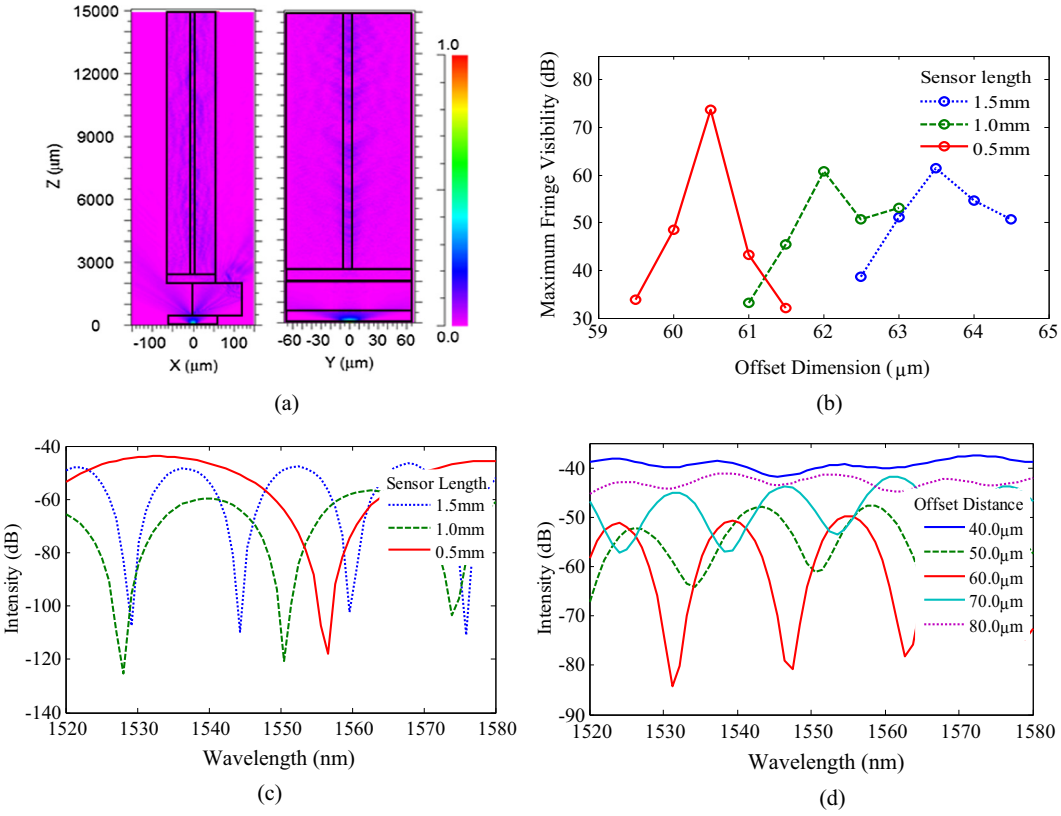

Fig. 2. (a) Simulated field distribution along fiber structure from X-Z and Y-Z planes of the structure, (b) maximum fringe visibility at varying offset distance, (c) simulated spectra for sensors with optimum offset distance, and (d) simulated spectra at various offset distance for 1.5 mm sensor showing distinguishable fringe visibility even at large offset.

3. Fabrication process

There are four fabrication steps involved for this offset structure sensor which are shown in Fig. 3. The main process involved the fusion splicing which is done by using Fujikura FSM-60S fusion splicer. First, two set of SMF-CSF sections are prepared by automatic splicing between a SMF and a CSF sections. Next, a cleaved section of a CSF fiber is aligned with manual mode in x-direction at the optimum offset distance to one of the SMF-CSF section. In y-direction, these two sections are aligned centrally and should be seen as a straight fiber. Then, the two sections are spliced using pre-determined recipe; arc power = 50 units and arc duration time = 550 ms. The captured image of spliced offset section from the splicing machine is shown in Fig. 4. In the following step, the CSF offset section is cleaved under microscope (5 mm full scale, 0.1 mm smallest scale division) at desired sensor length. While the cleaver cover in open position, the required section B length is measured from the spliced offset point to the cleaver blade. Finally, the end-face of the offset CSF section is spliced with the other part of SMF-CSF section using the similar pre-determined recipe.

4. Experimental results and discussion

The experimental setup to test the sensor response towards refractive index changes is shown in Fig. 5. It consists of a C-band broadband light source (Photonic P-ASE-C-20-NF-F/A) which is connected to the lead-in fiber of the sensor. The lead-out sensor fiber is connected to an optical spectrum analyzer (ANDO AQ6317B) which is used to monitor spectra changes due to RI or temperature changes.

For RI measurement, the sensor is tested with a set of RI liquids (Cargille Series AAA). We limit the refractive index range from 1.33 to 1.345 for the test as large wavelength shift (>10 nm) already achieved within this range. For each measurement, two drops of the RI liquid are applied on the sensor head using a pipette. The liquid is left to spread and stabilized after 1 minute before the sensor spectrum is recorded. The RI liquid is then cleaned delicately using alcohol before the next RI liquid (with increasing value) is applied. In order to avoid any influence of bent or stress during the experiment, the fiber is kept in straight condition with constant strain applied by sticky tapes on both sides of the sensor. The RI sensing experiment is carried out in a well-controlled temperature environment. The transmission spectra of 1.5 mm sensor tested with different RI liquid is shown in Fig. 6(a). A redshift response can be observed from spectra dip throughout the tested RI range. The linear fit of the dip wavelength shifts for different RI as shown in Fig. 6(b) suggests the sensitivity of 750 nm/RIU has been achieved. As the surrounding RI is increasing, the effective refractive index of the gap modes outside the CSF will increase while the effective refractive index of CSF modes is unchanged. Consequently, the difference of effective refractive index between the CSF modes and the gap modes will decrease, and therefore, an increase of FSR. The direction of wavelength shift (either redshift or blueshift) in RI sensing depends on the excited modes which has been demonstrated in similar mechanism of long period fiber grating (LPFG) [22]. For our case, we expect higher order modes are excited in

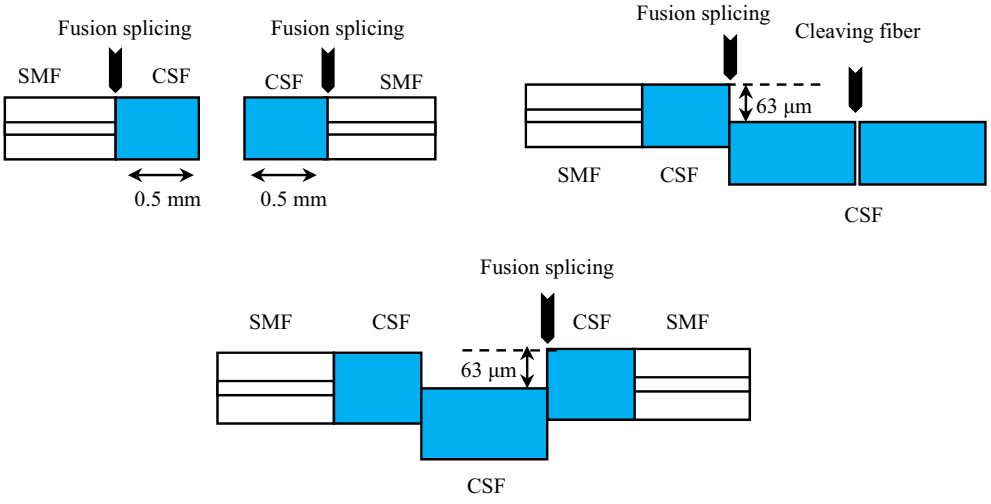

Fig. 3. Steps involve during fabrication of proposed sensor.

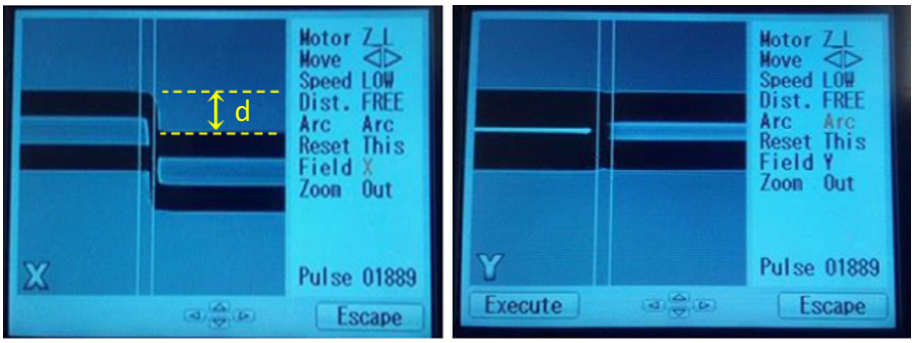

Fig. 4. Recorded image from splicing machine showing an offset splicing between two CSFs from x-direction (left) and y-direction (right).

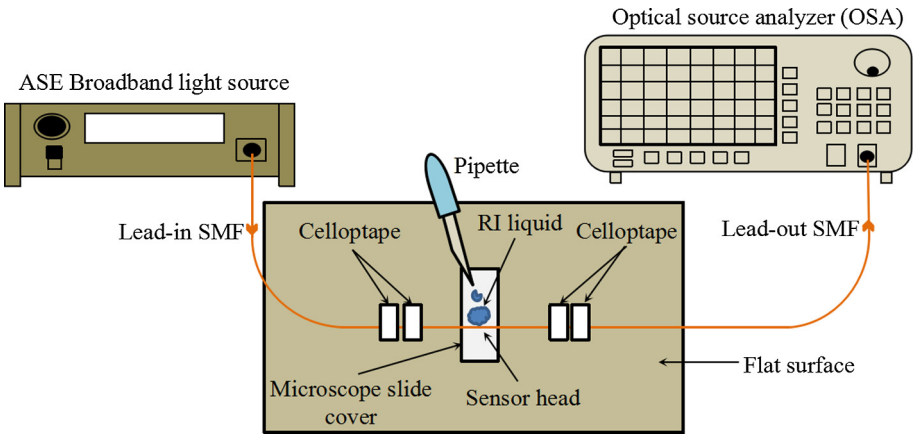

Fig. 5. Schematic diagram of RI measurement setup.

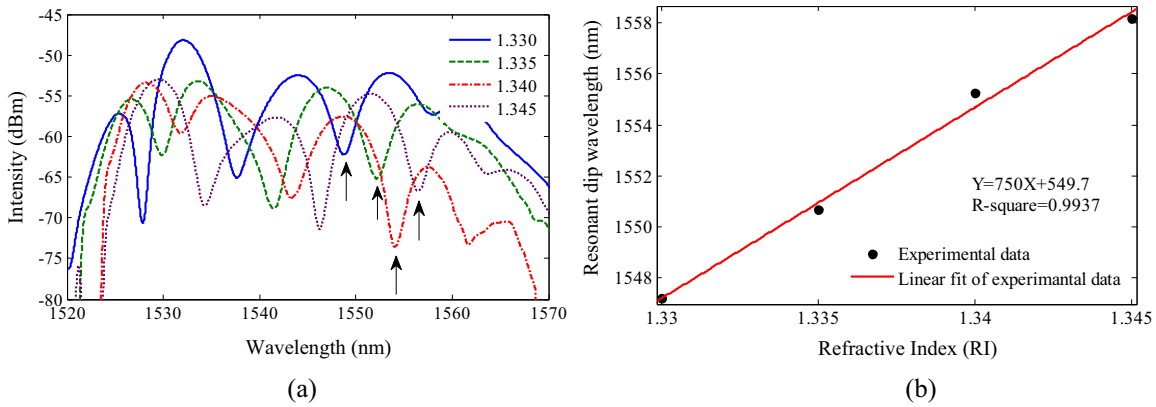

Fig. 6. (a) Transmission spectra shift of 1.5 mm length sensor tested with different RI liquids, (b) refractive index response of the proposed sensor monitored from the dip wavelength changes.

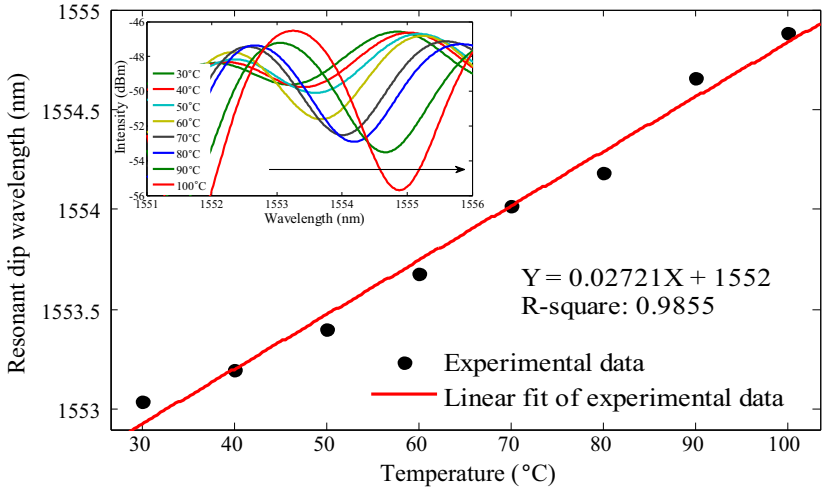

Fig. 7. Temperature response of the proposed sensor monitored from the dip wavelength changes (shown by the inset).

both CSF and gap due to the attained response. Similar characteristic has been reported in other cited works as well [7,15,16].

Measurement of temperature response of the sensor is carried out inside a dry heat oven (Venticell) for temperature range between 30 °C and 100 °C with increment of 10 °C. Fig. 7 shows the spectral response of selected dips corresponding to different oven temperature. While the inset shows the full spectra of the sensor, indicating more dips are available with spacing ~6 nm due to the lower surrounding refractive index of air. As the temperature increases, the dip wavelengths are increased with the sensitivity of 27.21 pm/°C. Thermo-optics coefficient (TOC) is the dominant factor that determines temperature sensitivity of the sensor. Supposed, TOCs of silica fiber and air are $8.5 \times 10^{-6}\,K^{-1}$ and $-9 \times 10^{-7}\,K^{-1}$, respectively, an increase of temperature will

Table 2
Comparison between the available techniques in fiber MZI sensor in terms of the length, RI sensitivity and temperature sensitivity.

Techniques	MZI length	RI sensitivity	Temperature sensitivity
Fiber taper [5]	15 mm	1656.35 nm/RIU	–
Thinned fiber taper [6]	5 mm	2210.84 nm/RIU	9.42 pm/°C
Fiber core mismatched [7]	35 mm	141 nm/RIU	–
Partially ablated fiber using laser (trench structure) [8]	80 μm	~10,000 nm/RIU	51.5 pm/°C
Partially ablated fiber using laser (trench structure) [9]	51 μm	−9370 nm/RIU	–
Partially ablated fiber using laser (air hole structure) [10]	10 μm	–	44.1 pm/°C
Peanut shape structure [11]	42.5 mm	204.98 extinction ratio/RIU	18.1 pm/°C
Collapsed region of PCF [12]	1.2 mm	46.5 nm/RIU	22 pm/°C
Collapsed region of PCF with tapered MZI [13]	20 mm	1600 nm/RIU	8.49 pm/°C
Small offset (evanescent field) [14]	66 mm	−26.22 nm/RIU	46.5 pm/°C
Small offset (evanescent field) [15]	36 mm	13.76 nm/RIU	46.2 pm/°C
Small offset (evanescent field) with tapered MZI [16]	30 mm	78.7 nm/RIU	–
Large offset (direct interaction) [17]	0.414 mm	3402 nm/RIU	–
Current work	1.5 mm	750 nm/RIU	27.21 pm/°C

result in increase of the difference of effective refractive index. Hence, redshift response of interference pattern may be observed. As expected, the attained temperature sensitivity is relatively low and comparable with other fiber interferometer sensor [11]. Temperature compensation scheme using fiber Bragg grating [14,15] written on the lead in/out fiber close to the sensor head may be applied if required. A limitation of transmission type interferometric fiber sensor is its sensitivity to bending which is hard to prevent, hence further works in developing suitable packaging is required so that the sensor could maintain straight position even in harsh environment. Furthermore, packaging is essential before sensor being applied the actual application in order to reinforce the core-offset sensor because glass fiber is known to be susceptible to breakage. The structure also has the potential to be developed as a temperature sensor by encapsulating high thermo-optic material in the offset region.

Table 2 compares the previously proposed fiber MZI techniques in terms of length, RI sensitivity and temperature sensitivity. As discussed previously, fiber tapers [5,6] and partially ablated fiber [8,9] structures have superior performance, however the requirement for special equipment to construct the structure may increase the fabrication cost. The achieved sensitivity of 750 nm/RIU is relatively much higher than that of the RI sensors that work based on core-offset evanescent field interaction [14–16]. Furthermore, the fabricated size of 1.5 mm is also smaller compared to that of similar sensors. Although the proposed sensor has a disadvantage in terms of size and performance compared with another direct interaction type sensor [17], the lower fabrication tolerance requirement may be attractive for diverse applications.

5. Conclusion

In conclusion, a simple, compact and high sensitivity core-offset CSF-based MZI fiber structure has been proposed and experimentally demonstrated. The sensor achieves high RI sensitivity of 750 nm/RIU for RI range between 1.33 and 1.345 and temperature sensitivity of 27.21 pm/°C for temperature range between 30 and 100 °C. Apart from high sensitivity of the sensor, the lower tolerance requirement of the offset distance simplifies the complexity encountered during fabrication process. The high performance of the sensor is desirable in many sensing applications including blood diagnosis, water quality control and food industries.

Acknowledgement

We wish to acknowledge for the support received from the Research University Grants (Reference No: 10H38 and 12J50) by Ministry of Education, Malaysia.

References

[1] A.I. Azmi, I. Leung, X. Chen, S. Zhou, Q. Zhu, K. Gao, P. Childs, G. Peng, Fiber laser based hydrophone systems, Photon. Sens. 1 (2011) 210–221.
[2] A.I. Azmi, D. Sen, W. Sheng, J. Canning, G.-D. Peng, Performance enhancement of vibration sensing employing multiple phase-shifted fiber Bragg grating, IEEE. J. Lightwave Technol. 29 (2011) 3453–3460.
[3] N.I. Ismail, N.H. Ngajikin, N. Fadzlina, M. Zaman, M. Awang, Resolution improvement in Fabry-Perot displacement sensor based on fringe counting method, Telkomnika 12 (2014) 811–818.
[4] J. Zhou, Y. Wang, C. Liao, B. Sun, J. He, G. Yin, S. Liu, Z. Li, G. Wang, X. Zhong, J. Zhao, Intensity modulated refractive index sensor based on optical fiber Michelson interferometer, Sens. Actuat. B: Chem. 208 (2015) 315–319.
[5] T.K. Yadav, R. Narayanasmawy, M.H.A. Bakar, Y.M. Kamil, M.A. Mahdi, Single mode tapered fiber optic interferometer based refractive index sensor and its application to protein sensing, Opt. Exp. 22 (2014) 22802–22807.
[6] J. Yang, L. Jiang, S. Wang, B. Li, M. Wang, H. Xiao, Y. Lu, H. Tsai, High sensitivity of taper-based Mach – Zehnder interferometer embedded in a thinned optical fiber for refractive index sensing, Appl. Opt. 50 (2011) 5503–5507.
[7] Y. Ma, X. Qiao, T. Guo, R. Wang, J. Zhang, Y. Weng, Q. Rong, M. Hu, Z. Feng, Mach-Zehnder interferometer based on a sandwich fiber structure for refractive index measurement, IEEE Sens. J. 12 (2012) 2081–2085.
[8] L. Zhao, L. Jiang, S. Wang, H. Xiao, Y. Lu, A high-quality Mach-Zehnder interferometer fiber sensor by femtosecond laser one-step processing, Sensors. 11 (2011) 54–61.
[9] Y. Wang, M. Yang, D.N. Wang, S. Liu, P. Lu, Fiber in-line Mach Zehnder interferometer fabricated by femtosecond laser micromachining for refractive index measurement with high sensitivity, J. Opt. Soc. Am. 27 (2010) 370–374.
[10] M. Park, S. Lee, W. Ha, D. Kim, W. Shin, I. Sohn, Ultracompact intrinsic micro air-cavity fiber Mach Zehnder interferometer, IEEE Photon. Technol. Lett. 21 (2009) 1027–1029.
[11] R. Huang, K. Ni, Q. Ma, X. Wu, Refractometer based on a tapered Mach Zehnder interferometer with peanut-shape structure, Opt. Laser. Eng. 83 (2016) 80–82.
[12] H. Gong, C. Chan, F. Zhang, C. Wong, X. Dong, Miniature refractometer based on modal interference in a hollow-core photonic crystal fiber with collapsed splicing, J. Biomed. Opt. 16 (2011) 2–5.
[13] C. Li, S. Qiu, Y. Chen, F. Xu, Y. Lu, Ultra-sensitive refractive index sensor with slightly tapered photonic crystal fiber, IEEE Photon. Technol. Lett. 24 (2012) 1771–1774.
[14] X. Yu, X. Chen, D. Bu, J. Zhang, S. Liu, In-fiber modal interferometer for simultaneous measurement of refractive index and temperature, IEEE Photon. Technol. Lett. 28 (2016) 189–192.
[15] Q. Yao, H. Meng, W. Wang, H. Xue, R. Xiong, B. Huang, C. Tan, X. Huang, Simultaneous measurement of refractive index and temperature based on a core-offset Mach-Zehnder interferometer combined with a fiber Bragg grating, Sens. Actuat. A: Phys. 209 (2014) 73–77.
[16] Y. Zhao, X.-G. Li, L. Cai, A highly sensitive Mach-Zehnder interferometric refractive index sensor based on core-offset single mode fiber, Sens. Actuat. A: Phys. 223 (2015) 119–124.
[17] D.W. Duan, Y.J. Rao, L.C. Xu, T. Zhu, D. Wu, J. Yao, In-fiber Mach-Zehnder interferometer formed by large lateral offset fusion splicing for gases refractive index measurement with high sensitivity, Sens. Actuat. B: Chem. 160 (2011) 1198–1202.
[18] T. Erdogan, Cladding-mode resonances in short and long period grating filters, J. Opt. Soc. Am. 14 (1997) 1760–1773.
[19] J. Fan, J. Zhang, P. Lu, M. Tian, J. Xu, D. Liu, A single-mode fiber sensor based on core-offset inter-modal interferometer, Opt. Comm. 320 (2014) 33–37.
[20] J.M. Senior, M.Y. Jamro, Optical Fiber Communications: Principle and Practice, Prentice Hall, third ed., 2009, pp. 217–233.
[21] Thorlabs.com, Datasheet Coreless Silica Fiber, 2017, pp. 9–10.
[22] X. Shu, L. Zhang, I. Bennion, Sensitivity characteristics of long-period fiber gratings, IEEE. J. Lightwave Technol. 20 (2002) 255–266.